Electronic supplementary Information (ESI)

Electrochemical oxygen activation driven by enamine-keto push-pull interactions in triazole-based covalent organic polymers

Surajit Samui[a†], Greesh Kumar[a†], Thakur Rochak Kumar Rana[b], and Ramendra Sundar Dey [a*]

[a]*Institute of Nano Science and Technology, Sector- 81, Mohali-140306, Punjab, India.*

[b]*Department of Chemistry, Indian Institute Institute of Technology, Powai, Mumbai-400076, India.*

Email: rsdey@inst.ac.in

† These authors contributed equally.

	with O_2 and wiberg bond index (WBI) indicating about bond strength with respect of each one.

Section-1: Materials and experimental section

Materials: Phenol, resorcinol, and hexamethylenetetramine were purchased from Loba Chemie, India. Trichloroacetic acid, dimethyl acetamide, mesitylene, dioxane, acetic acid, tetrahydrofuran, ethanol, and methanol were purchased from Spectro-chem, India. All these chemicals were used without further purification. The water used in all the experiments was purified through a Millipore system.

Synthesis of 2,4-dihydroxy-1,3,5-triformylcarbaldehyde (DHTA):

This compound was synthesized following the previously reported method.[1] In an oven dried 100 mL round bottom flask, 5.5 g (50 mmol, 1 eq.) of resorcinol and hexamethylenetetramine (110 mmol, 2.2 eq.) was taken followed by addition of 50 mL trichloroacetic acid at 0 ˚ C under argon atmosphere. Then, the mixture was heated to 130 ˚ C for 16 h followed by heating at 150 ˚ C at 3 h. Then 80 mL 3M HCl was added after cooling the solution to 100 ˚ C. Then, the solution was again heated to 105 ˚ C for another 30 min. After cooling to the room temperature, the solution was filtered followed by extraction with dichloromethane. Then, solution was dried over magnesium sulphate followed by filtration. Rotary induced evaporation led to the formation of off-white powder.

^{1}H NMR (400 MHz, DMSO-d_6) δ 10.25 (s, 1H), 10.08 (s, 2H), 8.38 (s, 1H). ^{13}C NMR (101 MHz, DMSO-d_6) δ 194.37, 190.40, 170.64, 141.09, 116.21, 110.46.

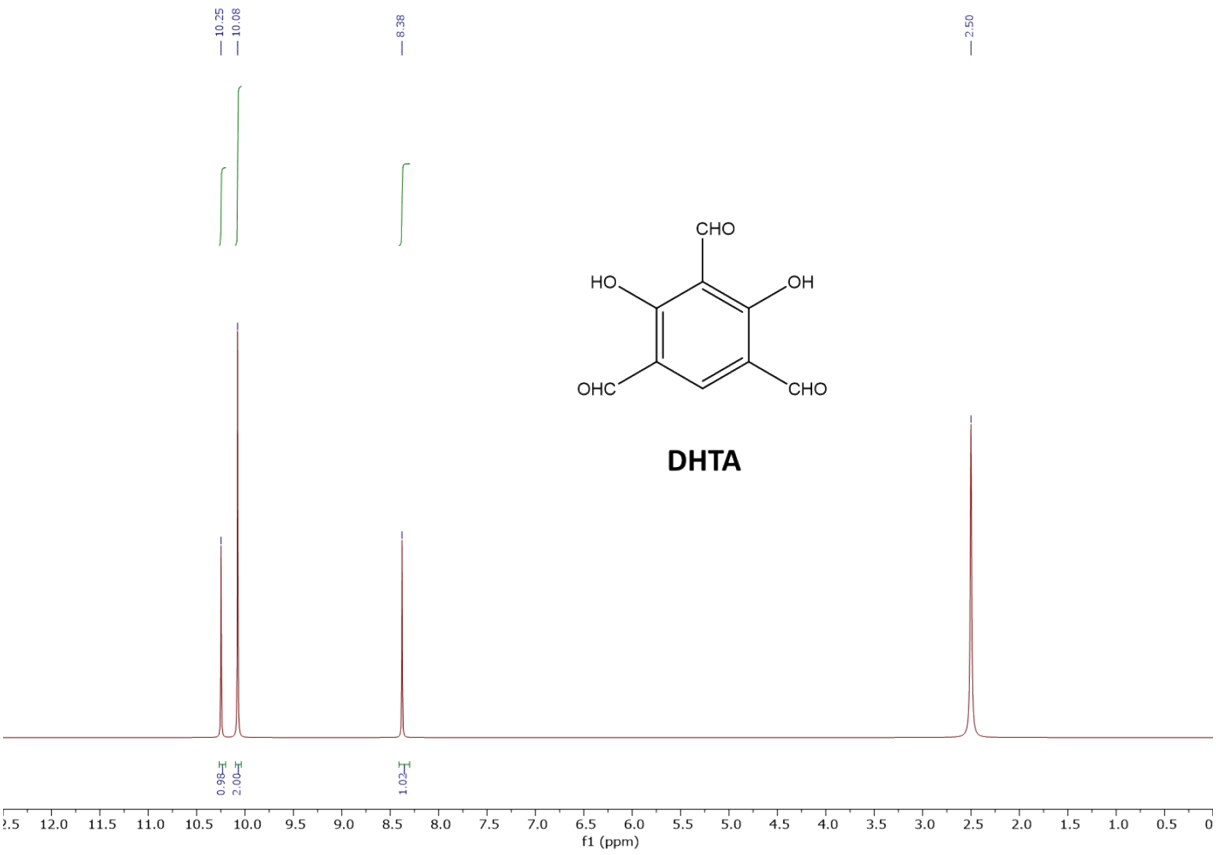
10.25
10.08
8.38
2.50
CHO
HO
OH
OHC
CHO
DHTA
0.98
2.00
1.03
f1 (ppm)

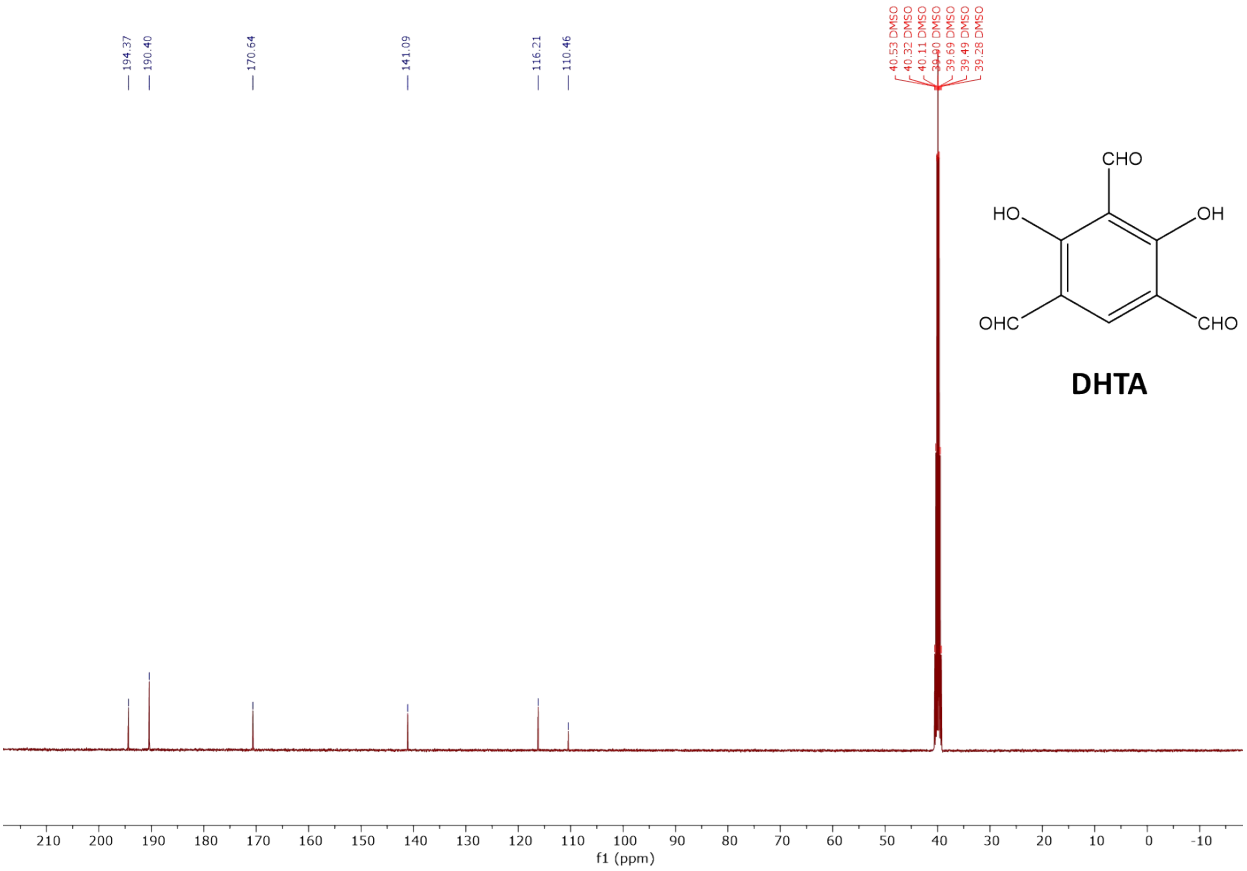
194.37
190.40
170.64
141.09
116.21
110.46
40.53 DMSO
40.32 DMSO
40.11 DMSO
39.90 DMSO
39.69 DMSO
39.49 DMSO
39.28 DMSO
CHO
HO
OH
OHC
CHO
DHTA
210 200 190 180 170 160 150 140 130 120 110 100 90 80 70 60 50 40 30 20 10 0 -10
f1 (ppm)

Synthesis of 2-hydroxy-1,3,5-triformylcarbaldehyde (HTA):

This compound was synthesized following the previously reported method.[2] In an oven dried 100 mL round bottom flask, 1.9 g (20 mmol, 1 eq.) of phenol and hexamethylenetetramine 5.9 g (42 mmol, 2.1 eq.) was taken followed by addition of 50 mL trichloroacetic acid at 0 ˚ C under argon atmosphere. Then, the mixture was heated to 120 ˚ C for 20 h followed by heating at 150 ˚ C at 30 min. Then 50 mL 3 M HCl was added after cooling the solution to 100 ˚ C. Then, the solution was again heated to 105 ˚ C for another 30 min. After cooling to the room temperature, yellow precipitate was filtered and washed thoroughly with cold ethanol to obtain pale yellow product.

^{1}H NMR (400 MHz, DMSO-d_6) δ 10.32 (s, 2H), 10 (s, 1H), 8.53 (s, 2H). ^{13}C NMR (50 MHz, DMSO-d_6) δ 192.18, 191.3, 166.49, 137.82, 128.72, 124.63.

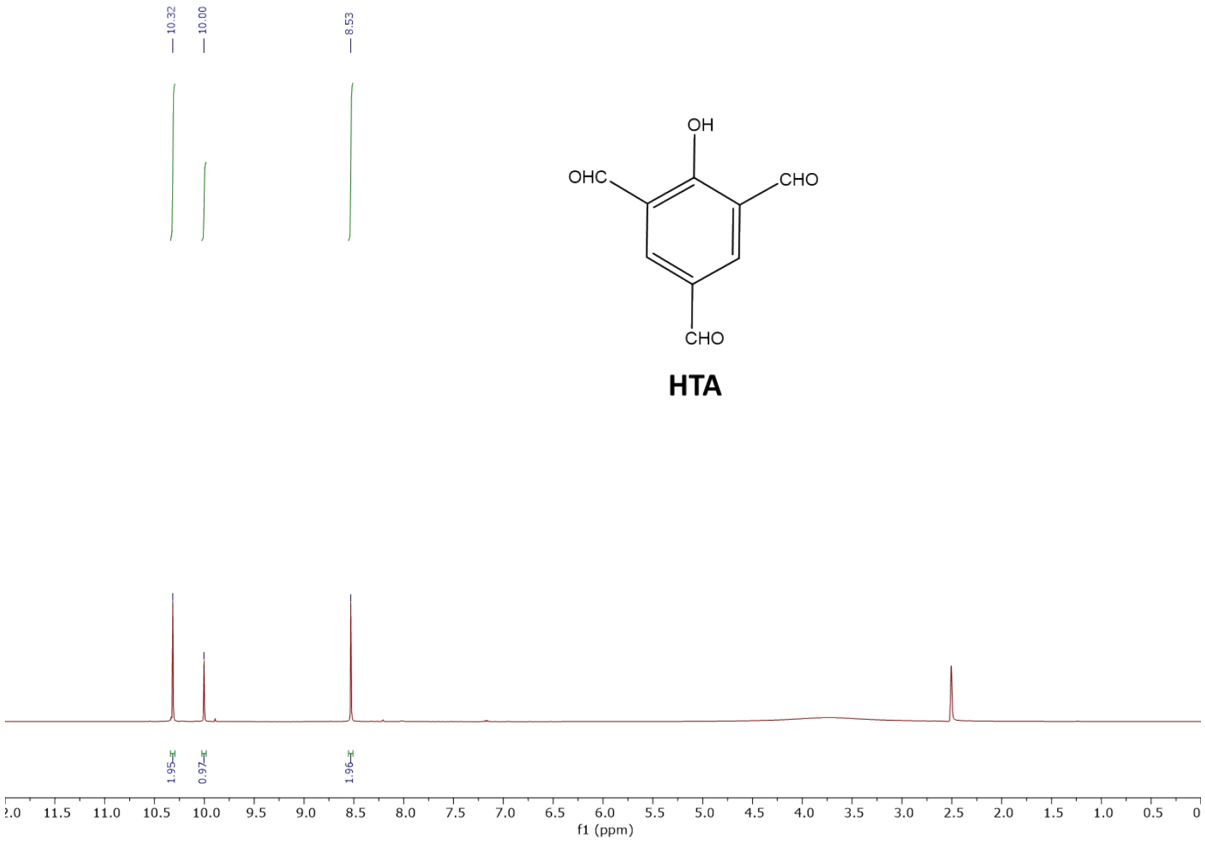

HTA

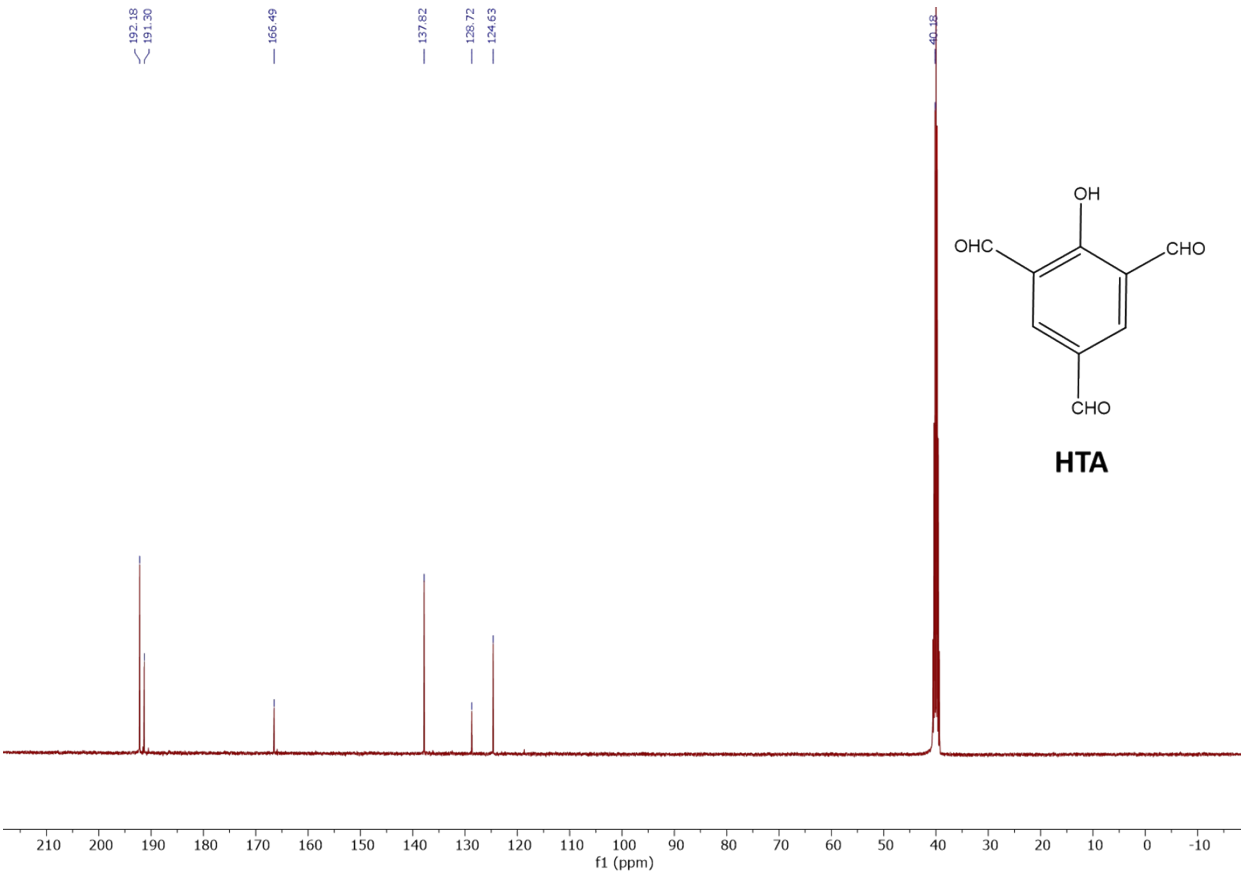
192.18
191.30
166.49
137.82
128.72
124.63
40.18
OH
OHC
CHO
CHO
HTA
210 200 190 180 170 160 150 140 130 120 110 100 90 80 70 60 50 40 30 20 10 0 -10
f1 (ppm)

Synthesis of RT-COP:

In a Schlenk tube, 2,4-dihydroxy-1,3,5-triformylcarbaldehyde (DHTA) (31 mg, 0.16 mmol) and 3,5-diamino-1,2,4-triazole (24 mg, 0.24 mmol) was taken followed by addition of 1 mL dimethyl acetamide, 1 mL mesitylene, 1 ml dioxane and 0.3 mL 6 M acetic acid. Then the mixture was sonicated for 30 min to get a homogeneous dispersion. Then, the tube was flash frozen using liquid N_2 followed by degassing using vacuum pump for three continuous cycles. Then the tube was kept at 120 ˚C in an oil bath for 3 days to obtain red precipitate powder. The powder was filtered and washed with methanol, THF followed by Soxhlet extraction with methanol for 2 days. Finally, the powder was collected and dried in an oven at 110 ˚ C.

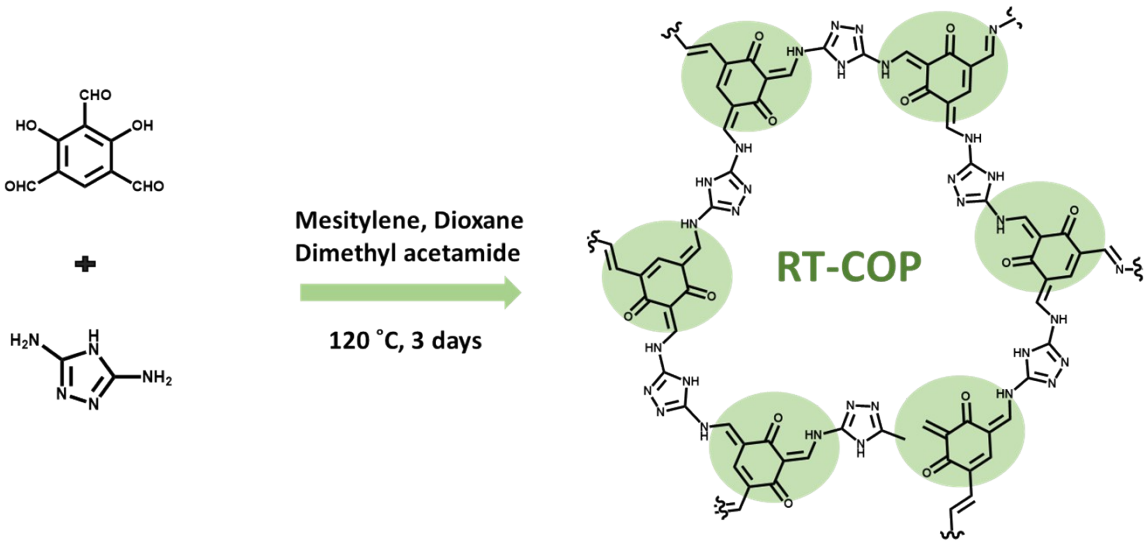

Synthesis of PT-COP:

In a Schlenk tube, 2-hydroxy-1,3,5-triformylcarbaldehyde (HTA) (35 mg, 0.2 mmol) and 3,5-diamino-1,2,4-traizole (30 mg, 0.3 mmol) was taken followed by addition of 0.5 mL dimethyl acetamide, 1 mL mesitylene, 1 ml dioxane and 0.3 mL 6 M acetic acid. Then the mixture was sonicated for 30 min to get a homogeneous dispersion. Then, the tube was flash frozen using liquid N_2 followed by degassing using vacuum pump for three continuous cycles. Then the tube was kept at 120 ˚C in an oil bath for 3 days to obtain yellow precipitate. The powder was filtered and washed with methanol, THF followed by Soxhlet extraction with methanol for 2 days. Finally, the powder was collected and dried in an oven at 110 ˚C.

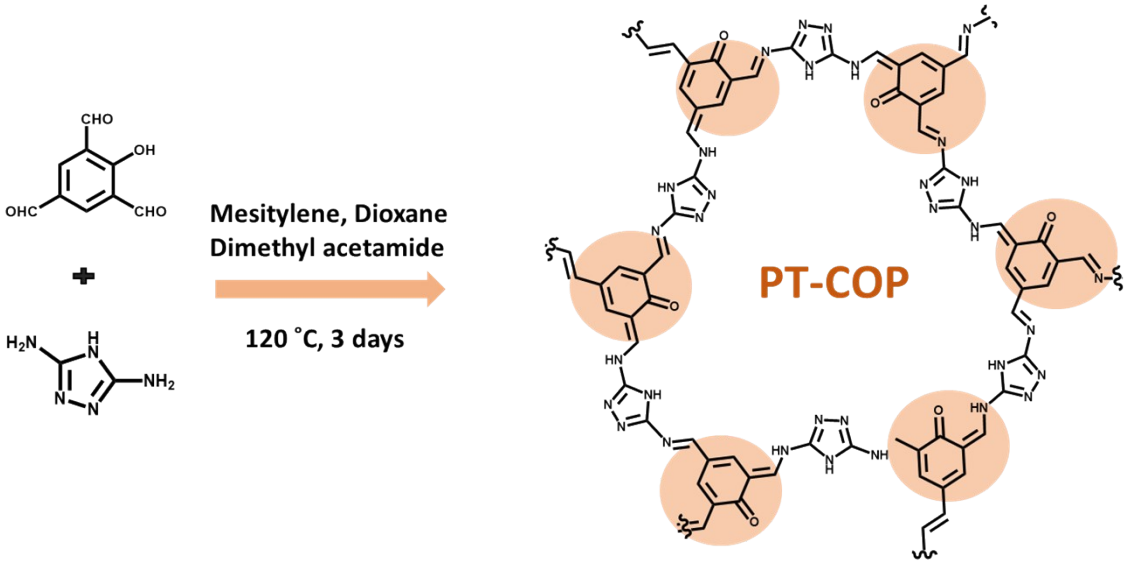

Instrumentation.

To analyze the crystallinity of covalent organic polymers, Powder X-ray diffraction (PXRD) analysis was carried out with Bruker D8 Advances instrument with Cu-Kα (λ = 1.5406 Å) radiation in the 2θ range from 5° to 60° with an acceleration voltage of 40 KV. To confirm structural analysis, Bruker NMR400 instrument was used. Field emission scanning electron microscope (SEM Jeol JSMIT300) was used to further characterize the detailed surface morphology. X-ray photoelectron spectroscopy (XPS) was performed to determine the bonding configuration and surface elemental composition using spectrometer (K-Alpha 1063) instruments in an ultrahigh vacuum chamber ($7X10^{-9}$ torr). All these spectra mentioned above of the synthesized materials were measured under ambient condition. All the condition is maintained throughout the experiment. Fourier transform Infrared spectroscopy (FT-IR) was carried out on FTIR BRUKER VERTEX 70 Sr. 2236 FTIR instrument at room temperature.

Electrode preparation:

The catalyst ink was prepared by dispersing 5 mg of RT-COP catalyst and 5 mg of activated carbon (acetylene black) in 1 mL of water and isopropanol (1:1) through ultrasonication for 45 minutes to create a homogeneous mixture. Before drop casting the material, the glassy carbon (GC) electrode, and rotating ring-disk electrode (RRDE) were thoroughly polished with 1, 0.3, and 0.05 μm alumina powder and rinsing ultrasonically in deionized (DI) water. The optimized mass of the synthesized catalyst ink was drop-cast onto the electrode surface and vacuum-dried for 12 hours. The catalyst inks for other PT-COP material were prepared using the same method. For comparison, the Pt/C (20 wt%) catalyst was prepared by dispersing 10 mg of Pt/C in a water and isopropyl alcohol mixture (1:1) containing 5% Nafion, followed by 45 minutes of ultrasonication. All electrochemical measurements were conducted at room temperature.

Electrochemical Measurements

Electrochemical characterizations were performed in a three-electrode cell setup using a Metrohm multichannel Autolab (M204) electrochemical workstation at room temperature. A catalyst coated rotating ring-disk electrode (RRDE; GC disk area 0.196 cm^2; Pt ring area 0.041 cm^2)

was used as working electrode, and Ag/AgCl (3 M KCl) as reference electrode. The graphite rod used as counter electrode in this study for ORR analysis. All the potentials were calibrated vs reversible hydrogen electrode (RHE) by using the equation:

$$E_{RHE}\ (V) = E_{Ag/AgCl\ (3\ M\ KCl)}\ (in\ V) + (0.059 \times pH) + 0.210\ V \qquad \text{Eq. (1)}$$

All the electrochemical measurements cyclic voltammetry (CV) and linear sweep voltammetry (LSV), chronoamperometry were carried out in 0.1 M KOH (pH >13) solution for ORR that was saturated with O_2 for 30 min prior to the reaction and also during the reaction O_2 saturation was maintained. As the system achieved equilibrium, the data was logged at the scan rate of 10 mV s^{-1}. During LSV test, the rotation speed of the working electrode (WE) was increased from 625 to 2500 rpm at the scan rate of 10 mV s^{-1}. The number of electrons transferred (n) per O_2 molecule, diffusion-limiting (J_L), and kinetic current densities (J_K) were calculated from the slopes (B) of the best linear fit lines of K-L plot using KL equation which is given by:

$$\frac{1}{J} = \frac{1}{J_L} + \frac{1}{J_K} = \frac{1}{B\omega^{\frac{1}{2}}} + \frac{1}{J_K} \qquad \text{Eq. (2)}$$

Where *j* is the measured current density, kinetic current densities (J_K), diffusion-limiting (J_L), and the number of electrons transferred (n) per O_2 molecule, ω is the angular velocity of the disk (ω = 2πN, N is the linear rotation speed), and B is the Levich slope.[3,4]

B is given by:

$$B = 0.62nFC_0\, D_0^{2/3} \vartheta^{-1/6} \qquad \text{Eq. (3)}$$

$$J_K = nFkC_0 \qquad \text{Eq. (4)}$$

Where *J* is the measured current density, J_L and J_K are the diffusion-limiting and kinetic current densities, n is the overall number of electrons transferred in oxygen reduction reaction, C_0 is the bulk concentration of O_2 in the solution, ϑ is the kinematic viscosity of the electrolyte (1.09×10^{-2} $cm^2\ s^{-1}$), D_0 is the diffusion coefficient of O_2 in 0.1 M KOH ($1.93 \times 10^{-5}\ cm^2\ s^{-1}$) and F is the Faraday constant (F = 96485 C mol^{-1}).

The number of electrons transferred (n) and H_2O_2 production yield is calculated from the RRDE measurement using equations:

$$n = 4 \times \frac{I\mathbf{D}}{I\mathbf{D} + \frac{I\mathbf{R}}{N}} \qquad \text{Eq. (5)}$$

$$\%H2O2 = 200 \times \frac{\frac{I\mathbf{R}}{N}}{\frac{I\mathbf{R}}{N} + I\mathbf{D}} \qquad \text{Eq. (6)}$$

where n is the number of electrons transferred (n) during the ORR process, I_R and I_D are the absolute value of the ring and disk currents, respectively. Here *N* is the current collection efficiency of the Pt ring (0.249 in this work).[1,2]

The electrochemical surface area (ECSA) of these COP materials were calculated by using a three-electrode system in alkaline media. To measure it cyclic voltammetry curve at different scan rates from 10 mV s^{-1} to 100 mV s^{-1} were taken in 0.1 M KOH electrolyte solution. The double layer capacitance (C_{dl}) of all these materials were measured through CV curves in a non-faradaic region with various scan rates (10, 20, 40, 60, 80, and 100 mV s^{-1}) by the following equation given below.

$$ECSA = \frac{C_{dl}}{C_s} \qquad Eq.\ (7)$$

Where C_s = 0.040 mF is the specific capacitance.

Section-2: Physical and electrochemical characterization

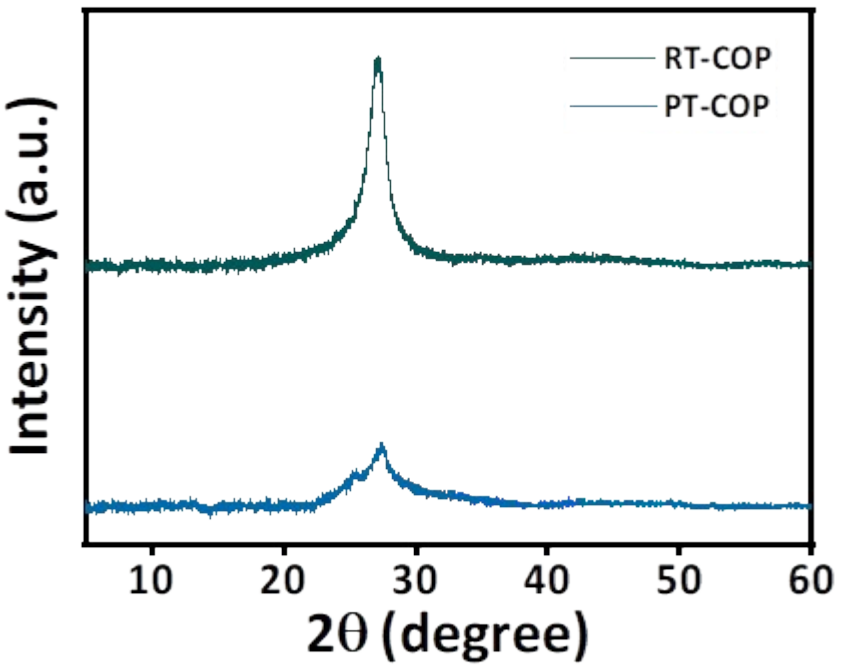

Fig. S1. Powder X-ray diffraction of RT-COP and PT-COP electrocatalyst.

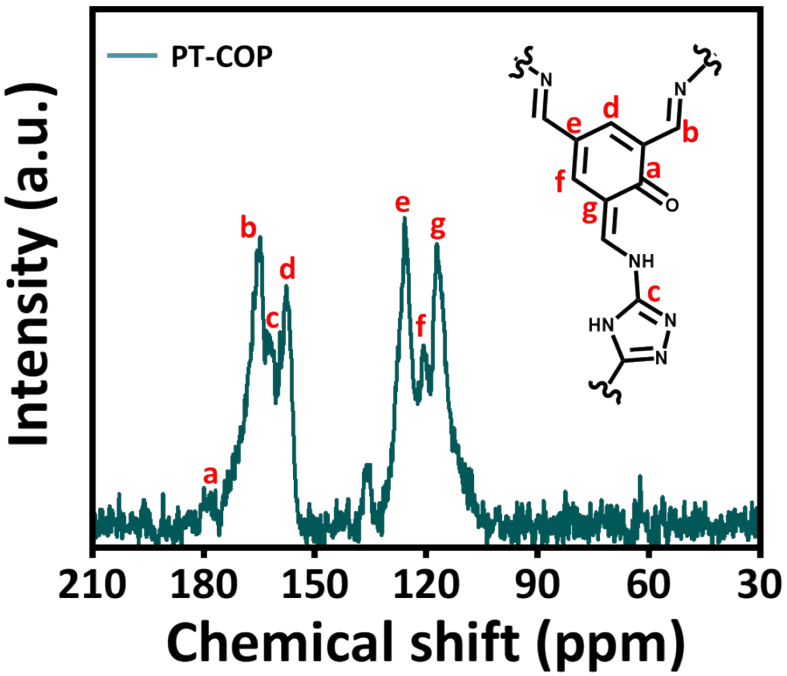

Fig. S2. ^{13}C Cross-polarization magic angle spinning solid state NMR spectroscopy data of PT-COP electrocatalyst.

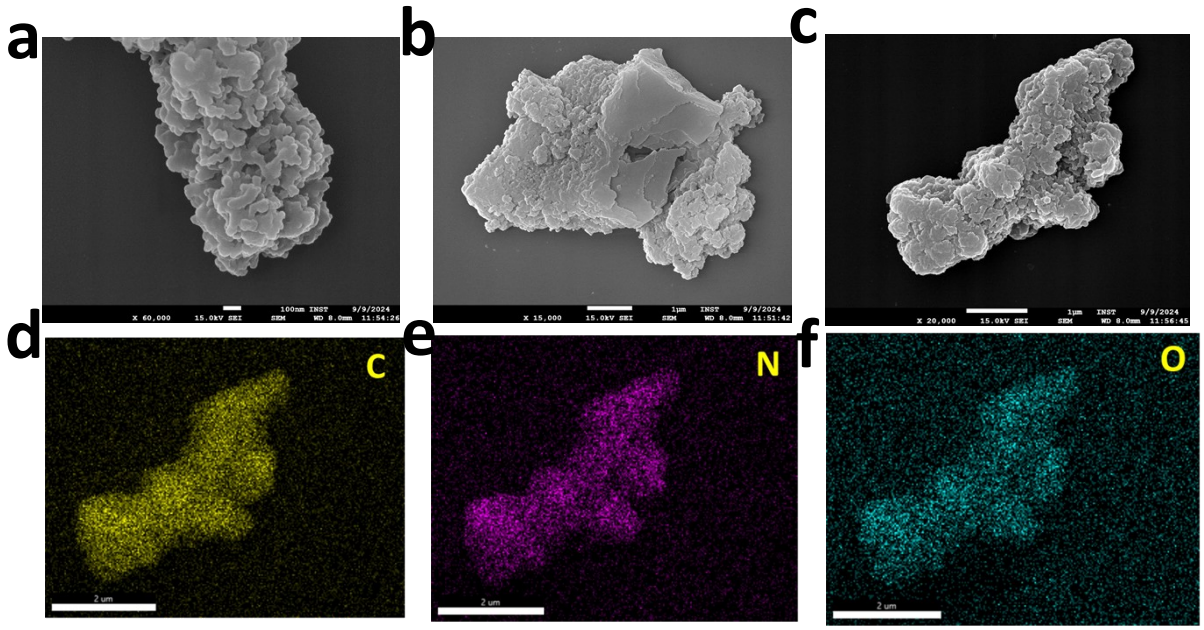

Fig. S3. (a-c) FESEM image of RT-COP material and (d-f) elemental mapping of C, N, O elements in RT-COP electrocatalyst.

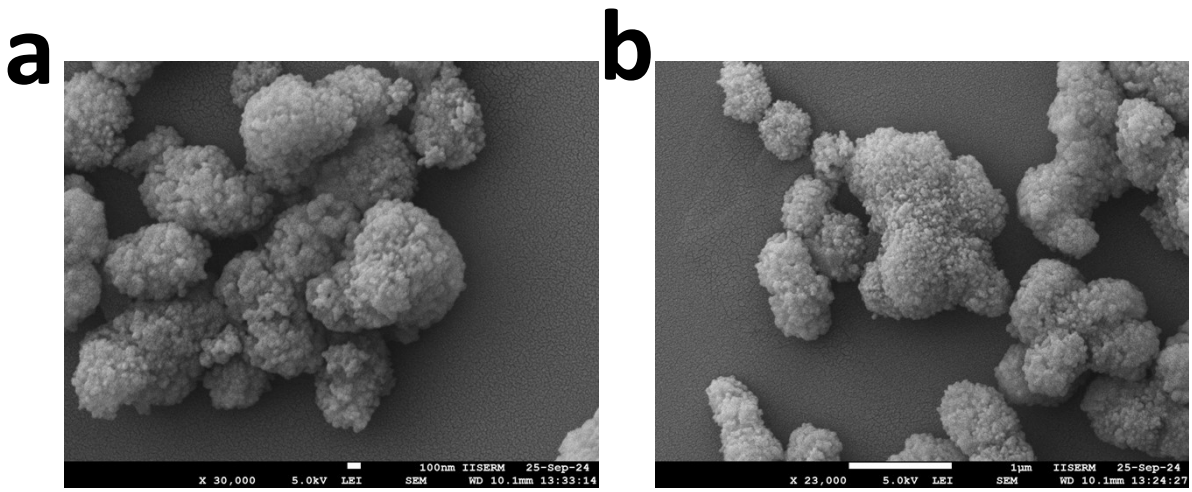

Fig. S4. (a-b) FESEM image of PT-COP material.

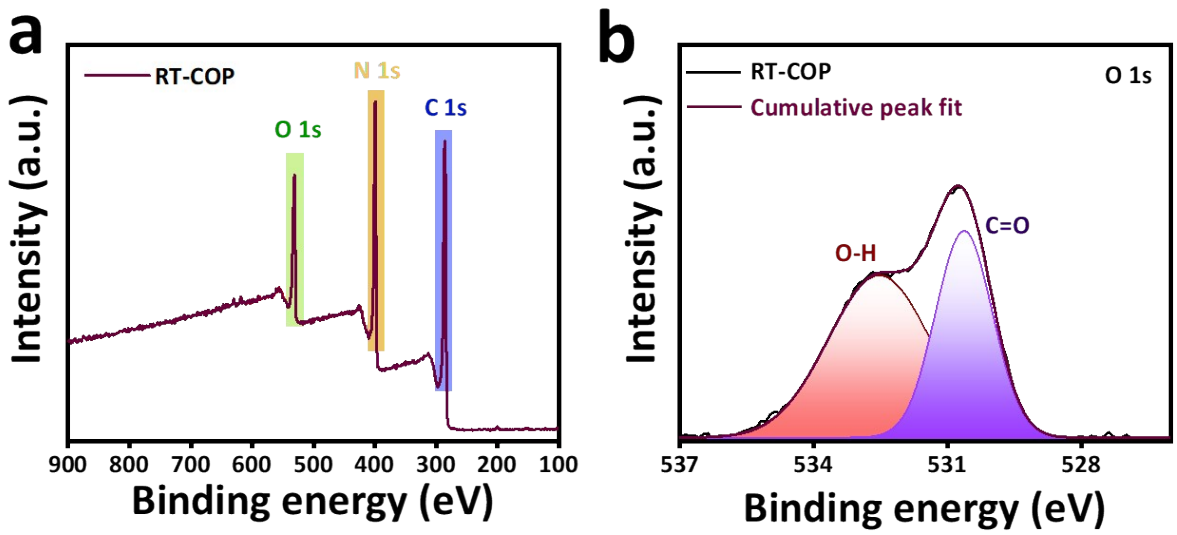

Fig. S5. (a) Full survey (b) High resolution XPS of O 1s of RT-COP material.

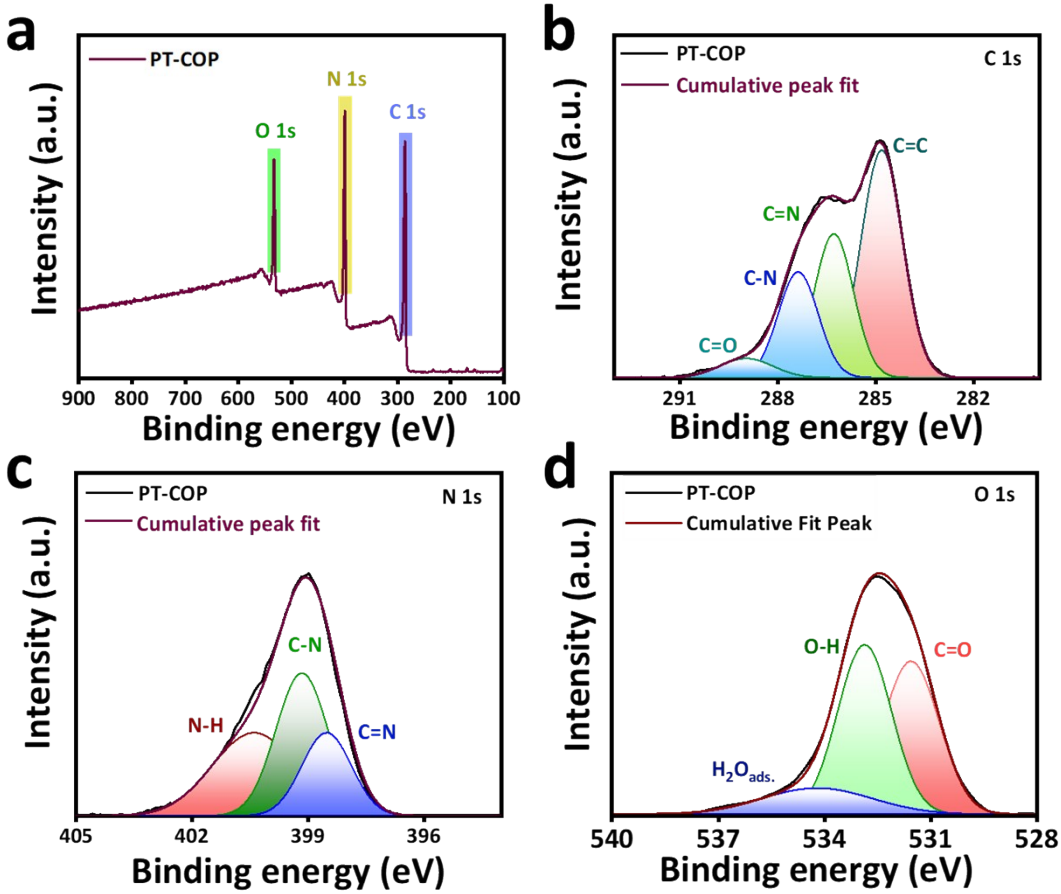

Fig. S6. (a) XPS Full survey. High resolution (b) C 1s (c) N 1s (d) O 1s spectrum of PT-COP

High resolution C 1s spectrum of PT-COP confirmed C=C, C=N, C-N and C=O functionality through deconvoluted peaks at 284.8 eV, 286.2 eV, 287.3 eV, 289 eV. Deconvoluted N 1s spectrum of PT-COP confirmed -NH, C-N, C=N functionality from the binding energies at 400.4 eV, 399.17 eV, 398.5 eV.

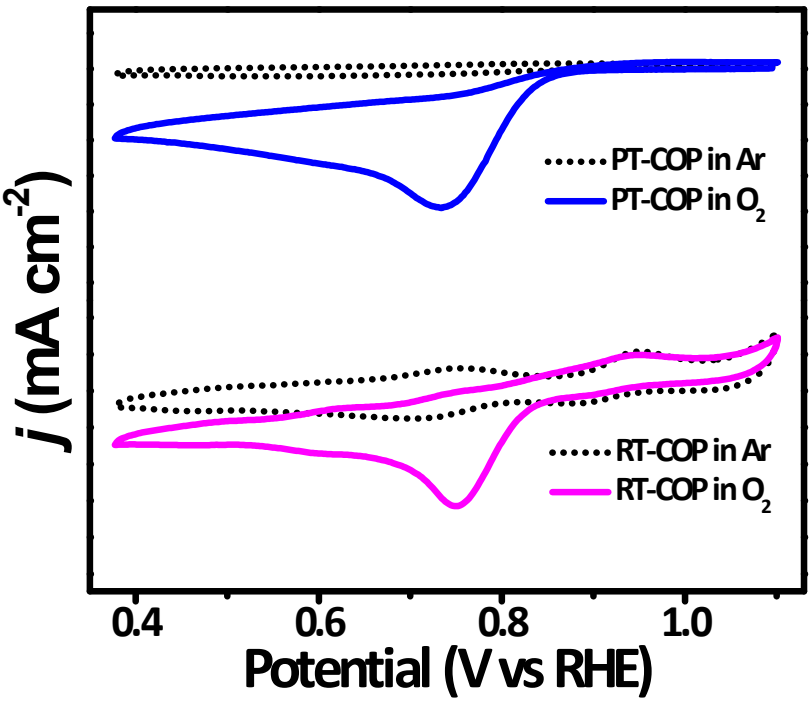

Fig. S7. Cyclic voltammetry (CV) analysis of RT-COP and PT-COP catalysts in the presence of Argon and O_2 gas saturated 0.1 M KOH electrolyte solution.

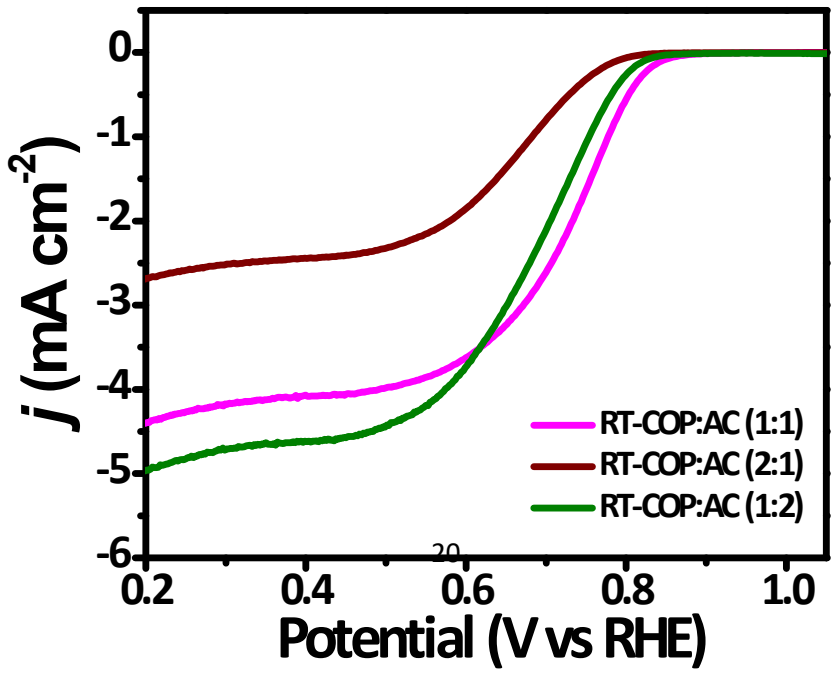

Fig. S8. LSV plots of RT-COP catalyst with different ratio of the activated carbon (AC) at 1600 rpm in alkaline solution.

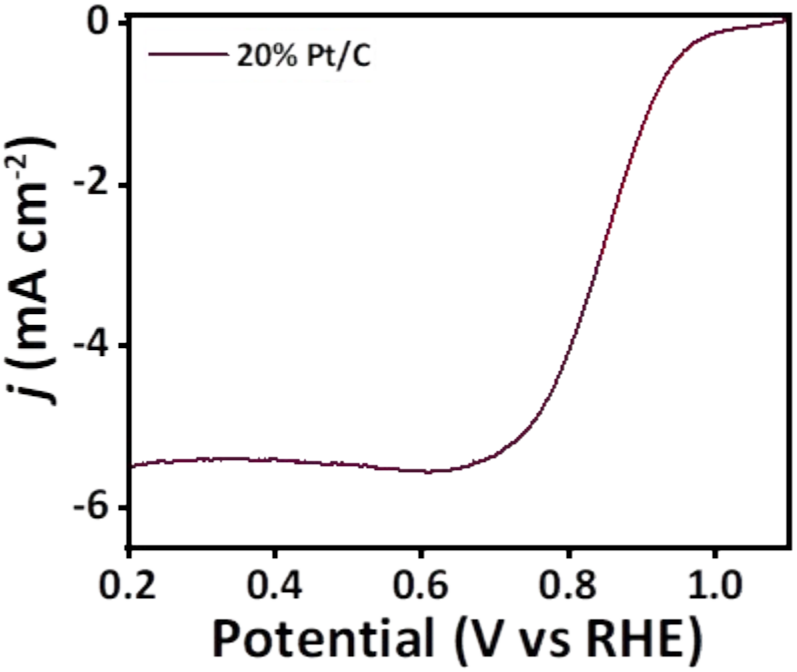

Fig. S9. LSV polarization curves of 20% Pt/C electrocatalyst

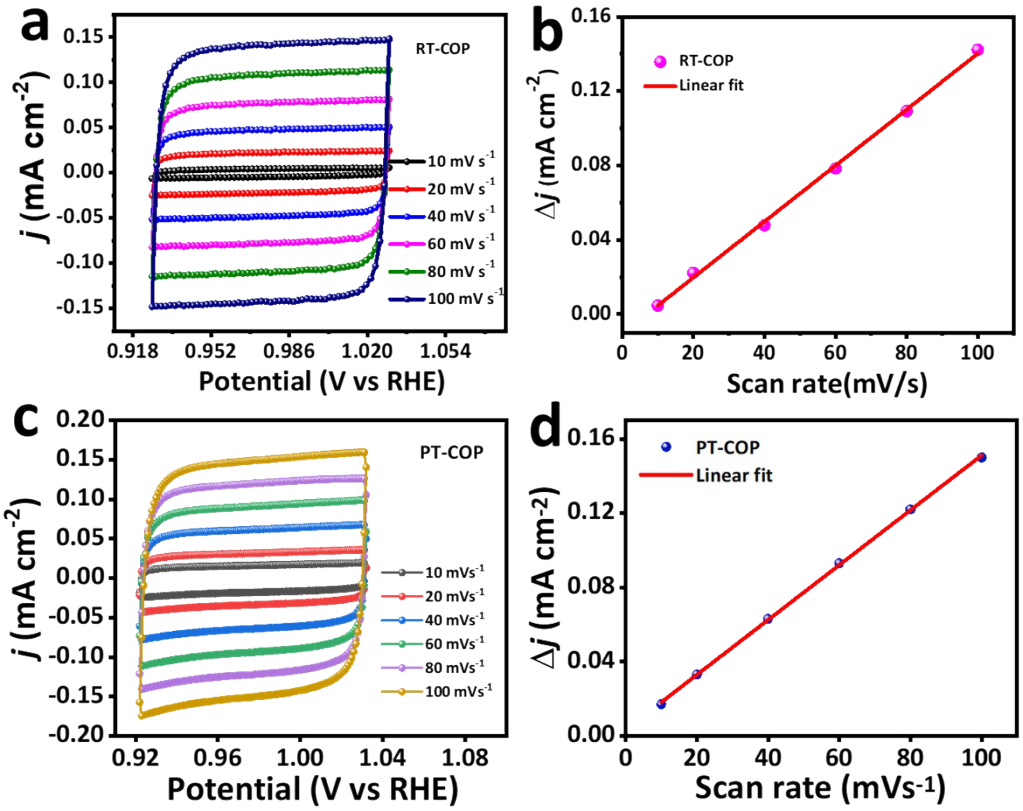

Fig. S10. Electrochemical active surface area analysis (a) CV curves of RT-COP at different scan rate (b) Linear fitting of capacitive currents of the RT-COP electrocatalyst vs scan rate (c) CV curves of PT-COP at different scan rate (d) Linear fitting of capacitive currents of the PT-COP electrocatalyst vs scan rate.

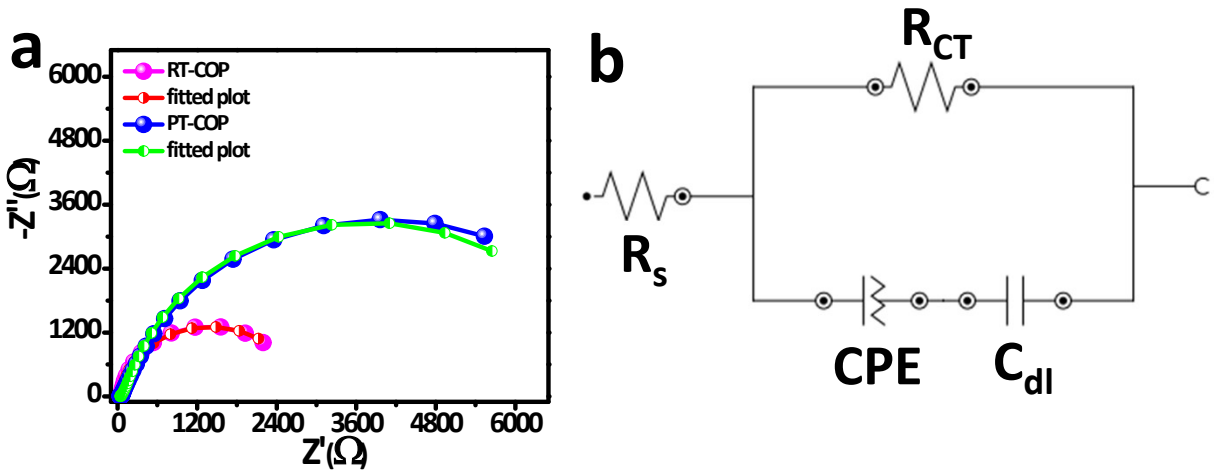

Fig. S11. (a) Electrochemical impedance spectroscopy (EIS) spectra of RT-COP and PT-COP materials; (b) equivalent fitted circuit of materials.

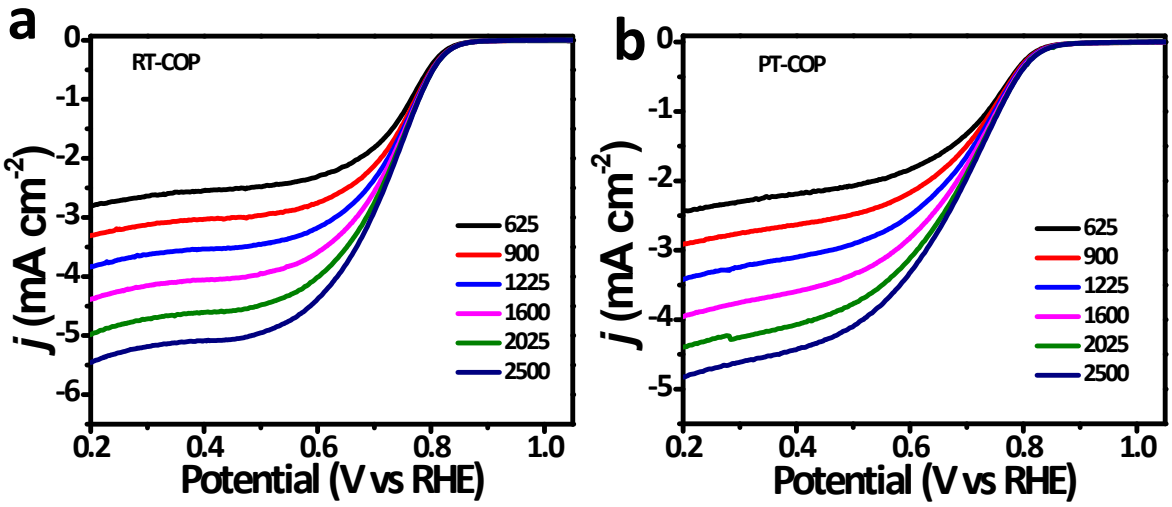

Fig. S12. LSV plots of (a) RT-COP and (b) PT-COP catalyst at different rotations (625-2500) in alkaline solution.

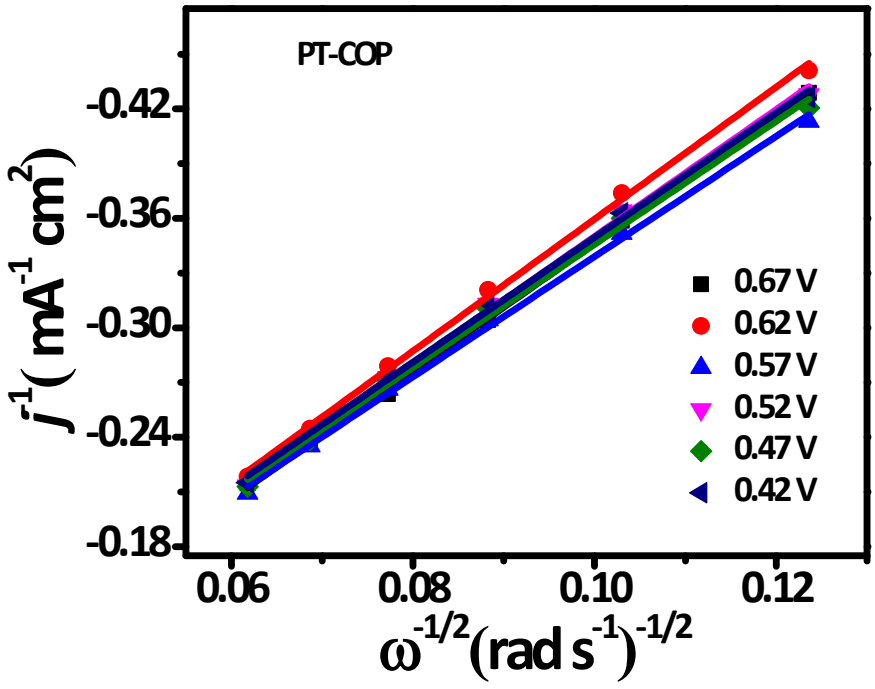

Fig. S13. (a) K-L plots of PT-COP catalyst at different potentials in alkaline solution.

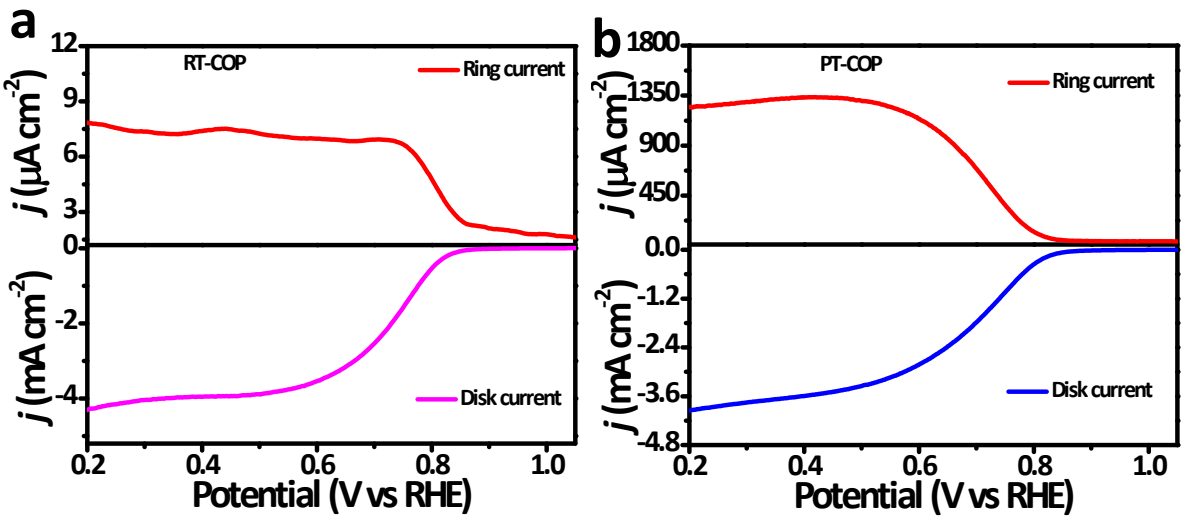

Fig. S14. Linear sweep voltammetry (LSV) polarization curve (a) RT-COP and (b) PT-COP catalysts at 1600 rpm in O_2 saturated 0.1 M KOH electrolyte solution with ring and disk current.

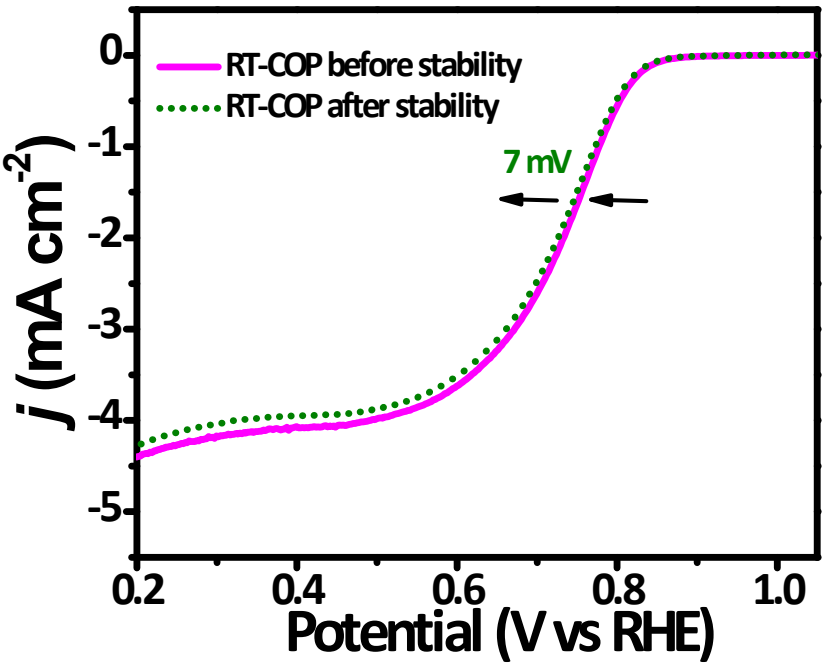

Fig. S15. Linear sweep voltammetry polarization curve before and after stability of RT-COP electrocatalyst.

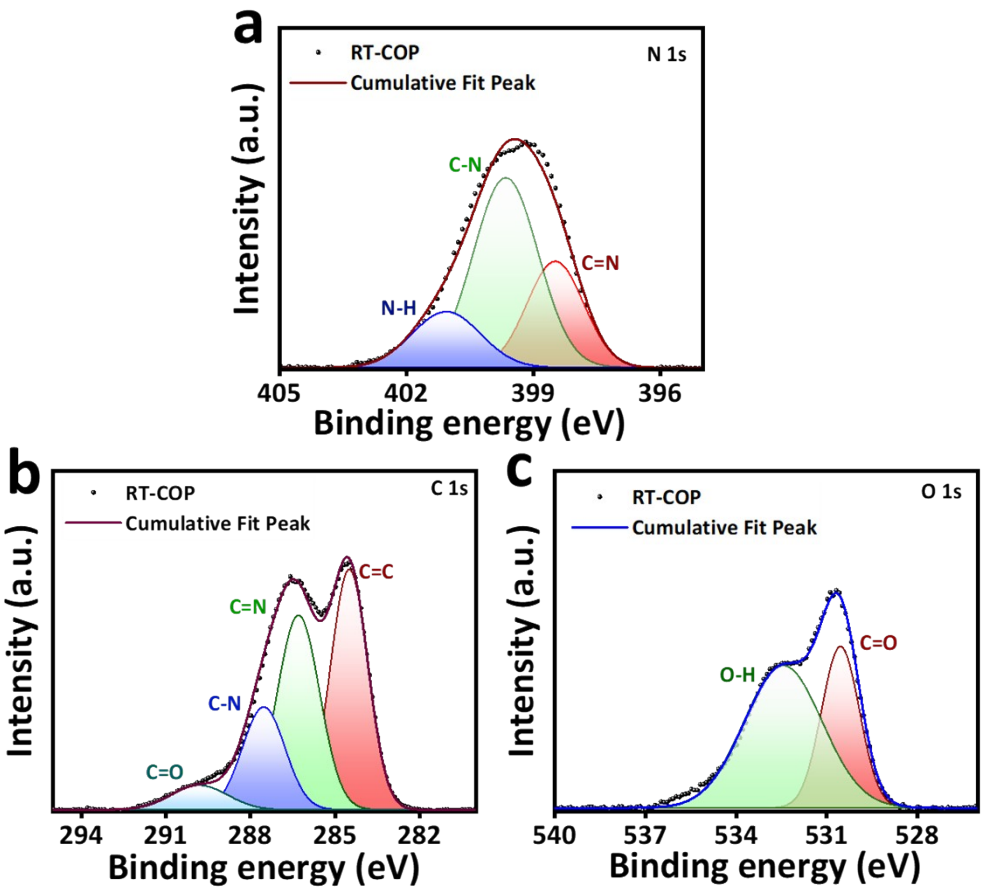

Fig. S16. After stability high XPS resolution (a) C 1s (b) N 1s (c) O 1s spectrum of RT-COP

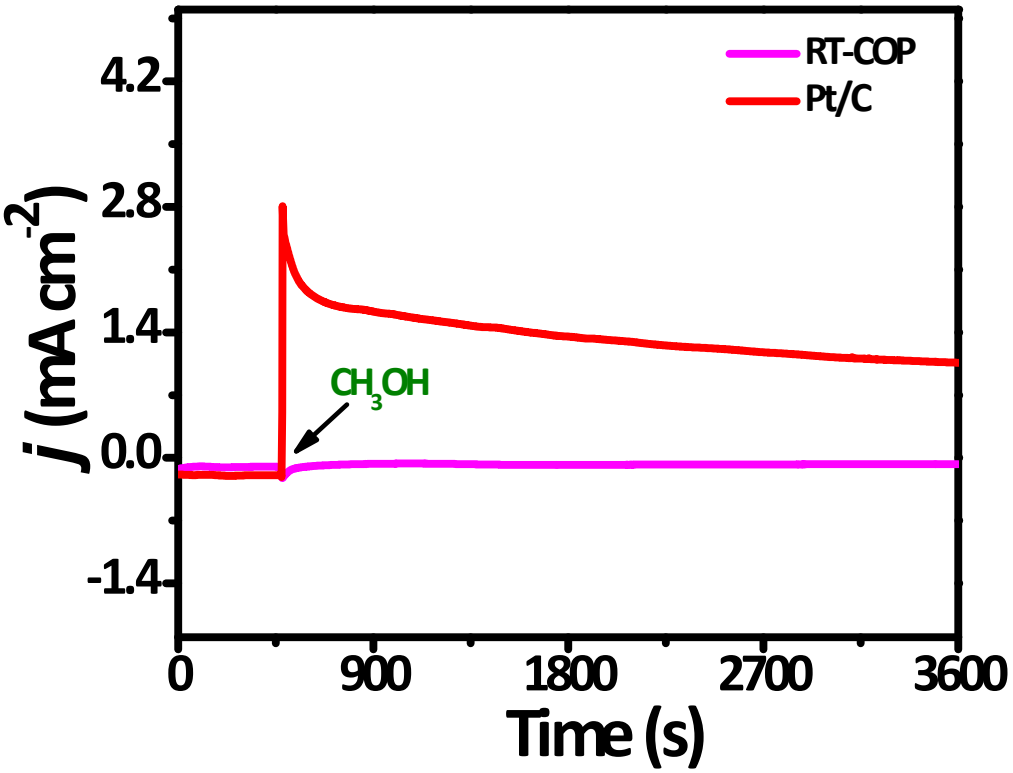

Fig. S17. Methanol cross over durability (i-t) curve of RT-COP in presence of 1 M methanol in O_2-saturated 0.1 M KOH solution and comparison with Pt/C catalyst.

The in-situ electrochemical Fourier transform infrared (FT-IR) spectroscopy of the RT-COP catalyst:

The in-situ FT-IR spectroscopic study for the ORR intermediate detection with RT-COP material have been performed in Argon and O_2 saturated alkaline media. The chronoamperometry technique was unutilized at different potentials (1.0, 0.90, 0.80, 0.70, 0.60, 0.50, and 0.40 V vs RHE) in Argon and O_2-saturated alkaline electrolyte. The in-situ FTIR spectra was recorded and intermediate products detected as explained in the main manuscript file. The peak intensity enhancement with the potential from 1.0 V to 0.4 V clearly indicates the formation of the water as a final product in the ORR catalysis.

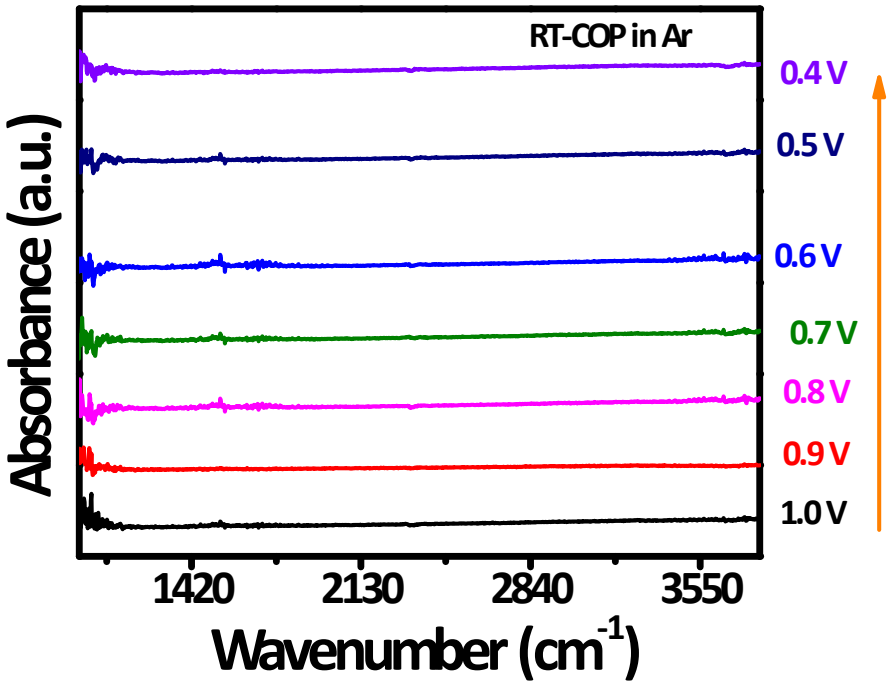

Fig. S18. In-situ FTIR spectra of RT-COP in argon-saturated electrolyte solution.

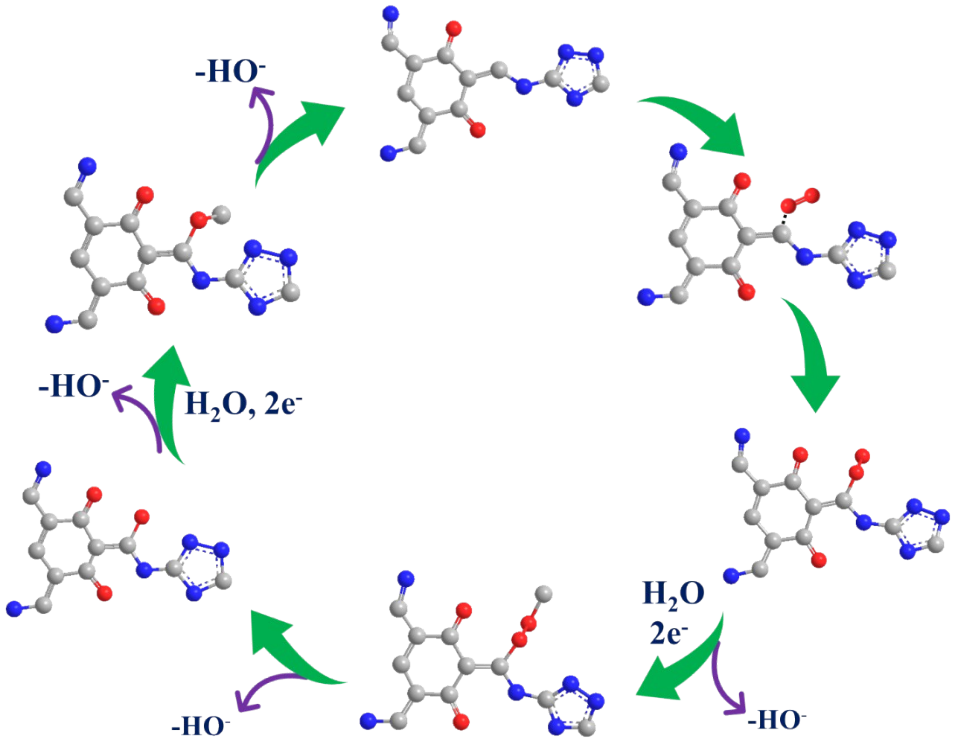

Fig. S19. Schematic representation of 4 e- pathway mediated oxygen reduction mechanism on RT-COP material.

Theoretical Study:

Methodology: In this study, all Density Functional Theory (DFT) calculations were performed using the Gaussian16 Rev B.01 quantum chemical software package.[3] Geometry optimizations were carried out employing the Grimme's dispersion-corrected B3LYP functional (B3LYP-D3).[4,5] To describe the atomic species, the 6-31G** basis set was used for carbon, hydrogen, nitrogen, and oxygen atoms. Frequency calculations were performed to confirm the nature of the stationary points on the potential energy surface (PES) and to provide thermal corrections to the free energy.[6,7] The optimized geometries were visualized using Chemcraft (version 1.6). Further analysis, including Natural Bond Orbital (NBO) and Wiberg Bond Index (WBI) calculations, was conducted at the B3LYP/Def2-TZVP level of theory, incorporating Grimme's GD3 dispersion corrections. The NBO analysis provided insights into the electronic structure and bonding characteristics, while the WBI analysis offered quantitative bond index values to assess bond orders. The zero-point vibrational energy (ZPVE) corrected complexation energies were calculated using the following expression:

$$\Delta E_{Comp}^{ZPVE} = \Delta E_{Comp}^{ZPVE} - E_{COP}^{ZPVE} - E_{O2}^{ZPVE} \qquad Eq.\,8$$

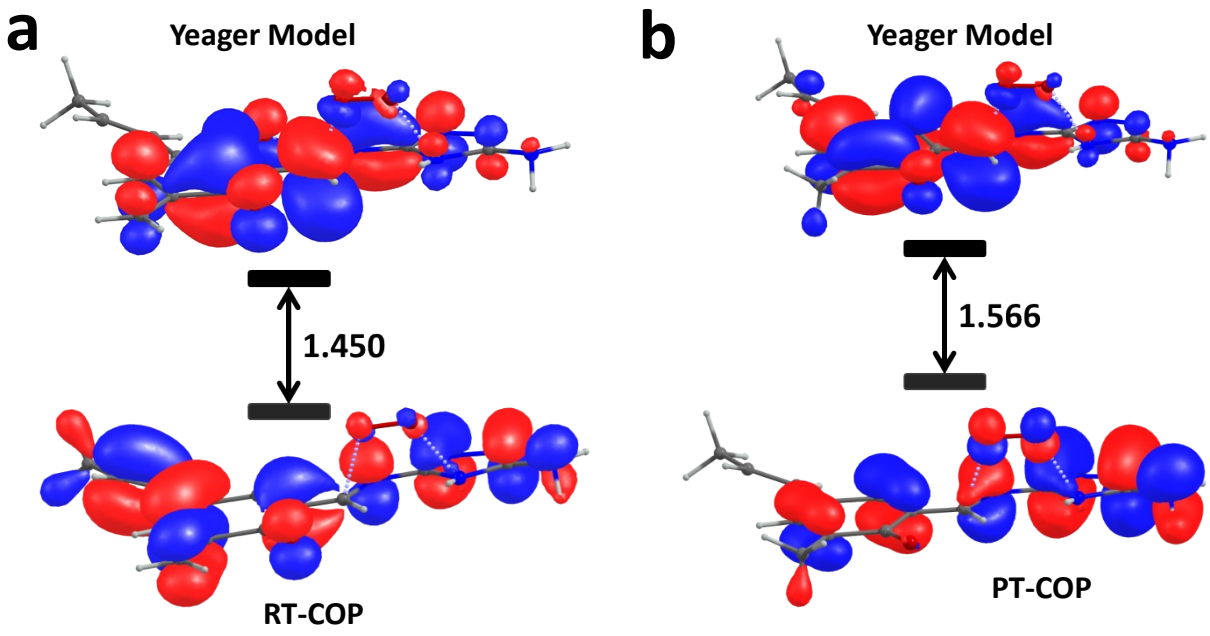

Fig. S20. HOMO-LUMO gap of (a) RT-COP and (b) PT-COP material with Yeager model [colour code: red- oxygen, blue- nitrogen, dark grey- carbon atoms]

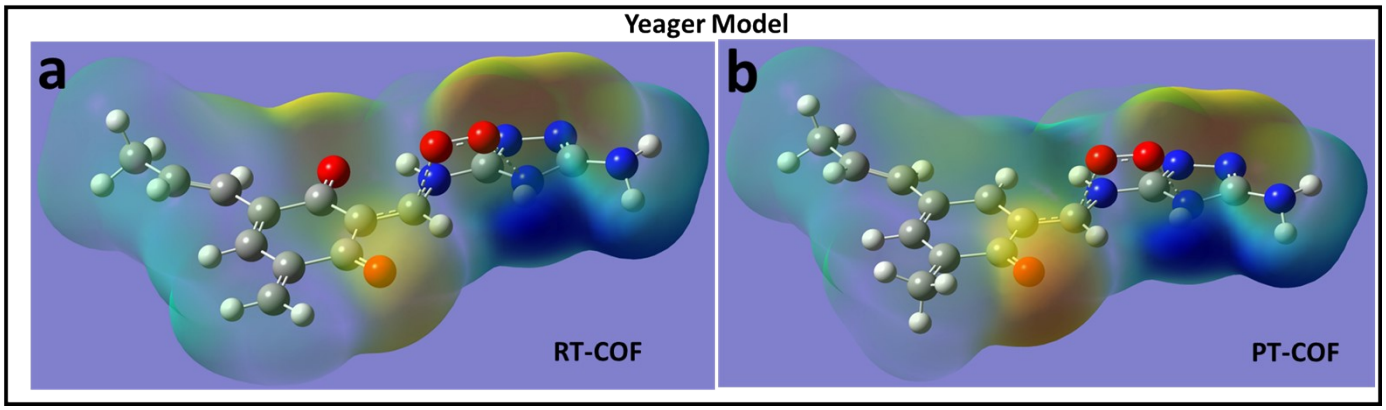

Fig. S21. Charge distributions on the atoms of (a) RT-COP and (b) PT-COP material with Yeager model [colour code: red- oxygen, blue- nitrogen, dark grey- carbon atoms]

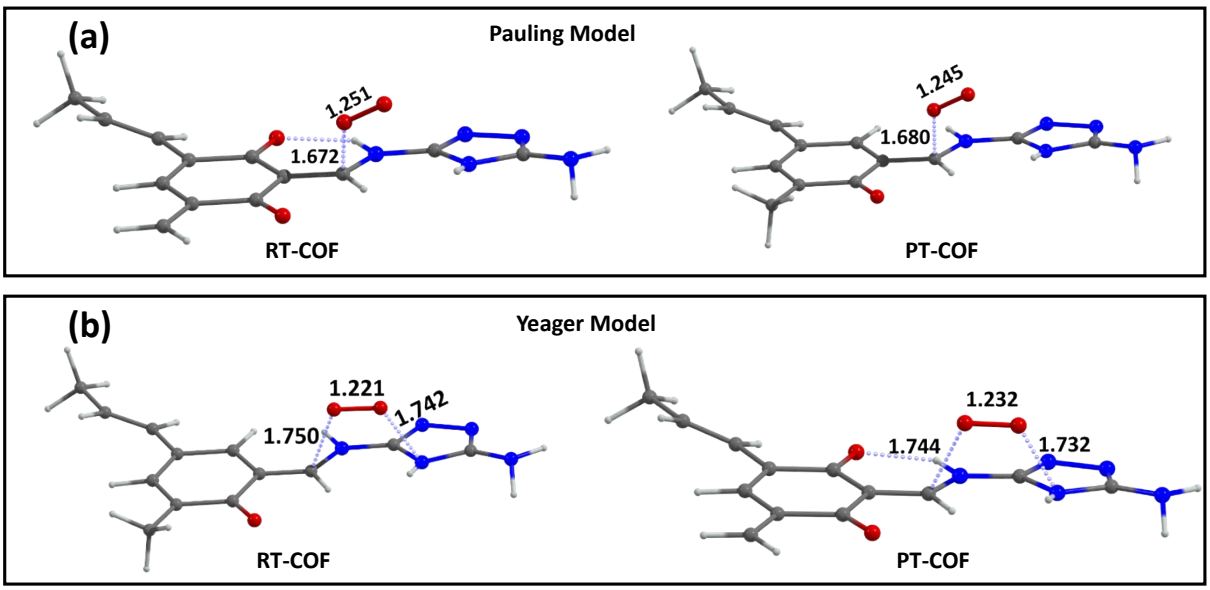

Fig. S22. 1:1 complex of (a) RT-COP and (b) PT-COP with dual binding models (Pauling and Yeager Model) interact with O_2, optimized at B3LYP/6-31g** level of theory. The bond length of the adsorbed O_2 is mentioned in Å for each complex, showing that O_2 bond length in these complexes has increased compared to that of the pure O_2 [colour code: red- oxygen, blue- nitrogen, dark grey- carbon atoms]

Table T1. Elemental analysis of RT-COP and PT-COP catalysts obtained from XPS analysis.

S No.	**Elements**	**RT-COP Catalyst**		**RT-COP Catalyst after stability**	**PT-COP Catalyst**
		Binding Energy (eV)	**Atomic (%)**	**Atomic (%)**	**Atomic (%)**
1.	Carbon (C)	285.95	59.36	58.17	61.24
2.	Nitrogen (N)	399.86	28.70	27.98	28.05
3	Oxygen (O)	531.73	11.94	13.85	10.71

Table T2. All the synthesized catalysts performances on the basis of electrocatalytic parameters for ORR

S. No.	Catalyst	Onset potential E_{onset} (V)	Half-wave potential $E_{1/2}$ (V)	Limiting current density J_L (mA cm^{-2})	Tafel slope (mV dec^{-1})
1	**RT-COP**	0.875	0.76	4.4	64
2	**PT-COP**	0.812	0.72	3.9	72
7	**Pt/C**	0.988	0.85	5.5	77

Table T3: The bond distances of interaction with binding site of RT-COP with O_2 and Wiberg bond index (WBI) indicating about bond strength with respect of each one.

Species	Bond Distances			Wiberg Bond Index (WBI)		
	O_1-O_2	C_N-O_1	C_C-O_2	O_1-O_2	C_N-O_1	C_C-O_2
One side	1.251	---	1.672	1.27	---	0.38
Both side	1.232	1.732	1.744	1.29	0.35	0.34

Table T4: The bond distances of interaction with binding site of PT-COP material with O_2 and Wiberg bond index (WBI) indicating about bond strength with respect of each one.

Species	Bond Distances			Wiberg Bond Index (WBI)		
	O_1-O_2	C_N-O_1	C_C-O_2	O_1-O_2	C_N-O_1	C_C-O_2
One side	1.245	---	1.680	1.29	---	0.32
Both side	1.221	1.742	1.750	1.32	0.31	0.30

References:

1 F. Cheng and J. Chen, *Chem. Soc. Rev.*, 2012, **41**, 2172–2192.

2 G. Kumar, R. Haldar, M. Shanmugam and R. S. Dey, *J. Mater. Chem. A*, 2023, **11**, 26508–26518.

3 M. J. Frisch, G. W. Trucks, H. B. Schlegel, G. E. Scuseria, M. A. Robb, J. R. Cheeseman, G. Scalmani, V. Barone, G. A. Petersson, H. Nakatsuji, X. Li, M. Caricato, A. V. Marenich, J. Bloino, B. G. Janesko, R. Gomperts, B. Mennucci, H. P. Hratchian, J. V. Ortiz, A. F. Izmaylov, J. L. Sonnenberg, D. Williams-Young, F. Ding, F. Lipparini, F. Egidi, J. Goings, B. Peng, A. Petrone, T. Henderson, D. Ranasinghe, V. G. Zakrzewski, J. Gao, N. Rega, G. Zheng, W. Liang, M. Hada, M. Ehara, K. Toyota, R. Fukuda, J. Hasegawa, M. Ishida, T. Nakajima, Y. Honda, O. Kitao, H. Nakai, T. Vreven, K. Throssell, J. A. Montgomery Jr., J. E. Peralta, F. Ogliaro, M. J. Bearpark, J. J. Heyd, E. N. Brothers, K. N. Kudin, V. N. Staroverov, T. A. Keith, R. Kobayashi, J. Normand, K. Raghavachari, A. P. Rendell, J. C. Burant, S. S. Iyengar, J. Tomasi, M. Cossi, J. M. Millam, M. Klene, C. Adamo, R. Cammi, J. W. Ochterski, R. L. Martin, K. Morokuma, O. Farkas, J. B. Foresman and D. J. Fox, Gaussian 16, Revision C.01, Gaussian, Inc., Wallingford CT, 2016.

4 Z. Shi, J. Zhang, Z. S. Liu, H. Wang and D. P. Wilkinson, *Electrochim. Acta*, 2006, **51**, 1905–1916.

5 A. D. Becke, *Phys. Rev. A*, 1988, **38**, 3098.

6 A. D. Becke, *J. Chem. Phys.*, 1997, **107**, 8554–8560.

7 J. Antony and S. Grimme, *Phys. Chem. Chem. Phys.*, 2006, **8**, 5287–5293.